

Supporting Information

**Asymmetric current-driven switching of synthetic antiferromagnets with Pt
insert layers**

Xiaotian Zhao, Wei Liu, Shangkun Li, Tingting Wang, Long Liu, Yuhang Song, Song*

Ma, Xinguo Zhao and Zhidong Zhang

This file include:

Section S1 The dominating role of lower magnetic layer and 5 nm Pt layer in current driven magnetization switching

Section S2 The switching phase diagrams (SPDs) affected by the tilted field.

Section S3 The influence of thickness of Pt insert layer on H_{DM} .

Section S4 The energy barrier for nucleation increased by AFM coupling.

Figure S1 The measuring of the effective field generated by spin-orbit torque using a harmonic method.

Figure S2 Channel conductivities of the Hall bars

Figure S3 The Hall signal reversal caused by in-plane magnetic field.

Figure S4 The switching phase diagram measured at magnetic field with out-of-plane component

Figure S5 MOKE microscope images with tilted domain walls

Figure S6 Measurement of H_{DM} for Ru(1)/Pt(50)/CoFe(0.41)/Pt(t_{Pt})/Ru(1.96)/Pt(2.3)

Figure S7 The influence of current duration on magnetization switching

Section S1 The dominating role of lower magnetic layer and 5 nm Pt layer in current driven magnetization switching

Limited by the quantity of sputtering guns, Pt is selected to be the top layer to keep strong enough perpendicular magnetic anisotropy. This Pt layer inevitably bring SOT to the FM layers. Here we prove that the SOT generated by this Pt layer can be ignored in the analysis of the current driven switching behavior. To separately investigate the transport and magnetic properties of the two FM layers in the SAF structure, two reference devices Ru(1)/Pt(5)/CoFe(0.41)/Pt(0.27)/Ru(1.96)/Pt(0.27)/ Pt(2) (device I) and Ru(1)/Pt(5)/Pt(0.27)/Ru(1.96)/ Pt(0.27)/CoFe(0.52)/Pt(2) (device II) were deposited and patterned into the shape same as the Hall bar used in the main text.

First, we measured the effective field generated by the electric current by harmonic Hall voltage measurements¹. Sinusoidal current with frequency $\omega/2\pi$ of 87 Hz is injected into the Hall-bar along x axis. The spin-Hall effect(SHE) generates spin accumulation σ along y axis at interface between the Pt layer and the CoFe magnetic layer with moment \mathbf{m} . This spin accumulation generates damping-like(DL) spin-orbit torque(SOT) along $\mathbf{m} \times (\boldsymbol{\sigma} \times \mathbf{m})$ and field-like SOT directed along $\mathbf{m} \times \boldsymbol{\sigma}$. The vibration of \mathbf{m} around the equilibrium position generated by the periodic SOT which contributes to the in-phase ω modulated (V_{ω}) and out-of-phase 2ω ($V_{2\omega}$) modulated Hall voltage. Under varying in-plane field along longitudinal direction (H_L) or transverse direction (H_T), the damping-like (H_{DL}) and field-like (H_{FL}) effective field generated by the current can be expressed by the formula:

$$H_{\text{DL(FL)}} = 2 \left(\frac{dV_{2\omega}}{dH_{\text{DL(FL)}}} \right) / \left(\frac{d^2V_{\omega}}{dH_{\text{DL(FL)}}^2} \right) \quad (1)$$

The in-plane field dependence of $V_{2\omega}$ is shown in Figure S1a-d. $V_{2\omega}$ varies linearly with $|H_{\text{L(T)}}| < 600$ Oe. The slope changes sign with the magnetization direction for the measurements under H_{T} , while under H_{L} the slope is positive for both magnetization directions, coincident with the expression of the field-like SOT and the damping-like SOT. The sign difference between device I and device II reflect the influence of reversed stacking sequence. In the measurement, the Hall voltage V_{H} contains contribution from anomalous Hall effect(AHE) and planar Hall effect(PHE), given by

$$V_{\text{H}} = I\Delta R_{\text{AHE}}\cos\theta + I\Delta R_{\text{PHE}}\sin^2\theta\sin 2\varphi \quad (2)$$

where the ΔR_{AHE} and ΔR_{PHE} are the saturation value of Hall resistance contributed by the AHE and SHE. We determine the ratio $\xi = \Delta R_{\text{PHE}}/\Delta R_{\text{AHE}}$ by the method developed by Woo et al ². Assuming the in-plane components of the magnetic moment and the external field have same direction, the contribution of the PHE can be shown by the difference between the V_{ω} values measured under in-plane field along $\varphi = 0^\circ$ and $\varphi = 45^\circ$, as shown in Figure S1e. Defining V_{ω} under in-plane field H along $\varphi = 0^\circ$ and $\varphi = 45^\circ$ as $V_{\omega}^0(H)$ and $V_{\omega}^{45}(H)$, the two signals follow the relationship

$$\frac{V_{\omega}^{45}(H) - V_{\omega}^0(H)}{V_{\omega}^0(0)} = \frac{\Delta R_{\text{PHE}}}{\Delta R_{\text{AHE}}} \cdot \frac{[V_{\omega}^0(0)]^2 - [V_{\omega}^0(H)]^2}{[V_{\omega}^0(0)]^2} \quad (3)$$

By linear fitting, the value of ξ is found to be 0.09 for the device I and 0.13 for the

device II. As the driving force of the magnetization switching in our work, the corrected effective damping-like (H_{DL}') effective field is expressed by the formula in ref³

$$H_{DL}' = -2 \frac{H_{DL} + 2\zeta H_{FL}}{1 - 4\zeta^2} \quad (4)$$

The results for H_{DL}' of the two devices are plotted in Figure S1f. The SOT transferring efficiency for device I is 1.25 Oe/10⁶Acm⁻² for device I and 0.45 Oe/mA⁻² for device II. The ratio of the effective fields in FM1 and FM2 is 2.76, which is close to the thickness ratio of the two Pt layers adjacent to the corresponding FM layers. To estimate the current distribution in the two Pt layers, two samples with the structure of Ru(1)/Pt(0 - 5)/Co₇₀Fe₃₀(0.41)/Pt(0.27)/Ru(1.96)/ Pt(0.27)/ Co₇₀Fe₃₀(0.52)/Pt(2) and Ru(1)/Pt(5)/Co₇₀Fe₃₀(0.41)/Pt(0.27)/Ru(1.96)/ Pt(0.27)/Co₇₀Fe₃₀(0.52)/Pt(0 - 2) respectively were deposited and patterned into the same Hall bars. Measured by a probe station, the channel conductivity versus the Pt layer thickness are plotted in Figure S2a, b. Linear fittings of the two curves show that the 5 nm (2 nm) Pt layer contribute to 52% (18.5%) of the total conductivity. The ratio between these two conductivities is 2.81, highly coincident with the result of the harmonic Hall voltage measurements, manifesting the bulk nature of the spin Hall effect. The effective field exerted to the FM layers is the main driving force in current-driven magnetization switching, the FM1 layer play the major role in the switching process.

Finally, in the measurement of the current driving switching loop in synthetic antiferromagnetic (SAF) structure, we find a reversal of Hall signal around $H_x = 1400$ Oe, as shown in Figure S3a. To investigate the origin of this phenomenon, we change to use a continuous current (I_{DC}) instead of the pulse to drive the switching loops. In

this mode, the Hall signal is influenced by the Joule heating effect. When I_{DC} is risen to ± 35 mA, a loss of perpendicular magnetic anisotropy (PMA) caused by the Joule heating effect⁴ contributes to the Hall signal in the form of the peaks around $I_{DC} = + 35$ mA and the dips around $I_{DC} = - 35$ mA, as shown in Figure S3b. Since whether the peak or the dip occurs is determined by the sign of $d\theta/d|I|$, it is clear that the z component of the FM layer that loses its PMA at $I_{DC} = \pm 35$ mA do not change sign along with the Hall signal. To check the relationship between this phenomenon and the magnetic properties of the single FM layer, the Hall signals of device I and II versus the in-plane field H_x are measured, as shown in Figure S3c. At $H_x = 0$, the device II has larger r_H value than device I, reflecting the thickness difference of the two FM layer. The anisotropy field H_k of the is estimated to be 5850 Oe, while that of the FM2 layer is around 3000 Oe. This difference in H_k mainly stems from the different buffering condition. Thus, along with increasing in-plane field, the difference value $|r_H^{FM2}| - |r_H^{FM1}|$ get smaller and change sign at the field $H_x = 1400$ Oe, coincident with the polarity switching of the Hall signal in current-driven magnetization switching. The polarity switching is just the net effect of the respective tilting of the magnetic moment in the two FM layers under in-plane field. This phenomenon is universal for SAF structures with different exchange coupling strength. We measured r_H as a function of H_x for SAF structure with $H_{ex} = 249$ Oe, 1037 Oe and 1874 Oe, corresponding to $t_{Ru} = 1.96, 0.86,$ and 0.31 nm, as shown in Figure S3d. The compensating points that have zero net Hall signal for all the three loops locate in a field range of $1200 \text{ Oe} < |H_x| < 1600 \text{ Oe}$. It means that this difference in PMA of FM1 and FM2 layers are general in

our samples. Meanwhile, it implies that the tilting of the two FM layers is a relatively independent process until the deterministic switching of magnetization. Combining this result with the discussion above, it is concluded that the current driving switching of the magnetization is mainly determined by the performance of the FM1 layer.

Section S2 The switching phase diagrams (SPDs) affected by the tilted field

To thoroughly exclude the possibility that the observed asymmetry in SPD comes from the out-of-plane component of the external magnetic field, we intently tilted the sample holder to induce the out-of-plane component. The result acquired at magnetic field with a small tilting angle $\theta > 0$ (the geometry is illustrated in Figure 1c) is shown in Figure S4. It is obvious that in high H_x range, all the boundary lines of the SPD are shifted towards right, just same as the single FM layer system. When $\theta < 0$, as shown in Figure S4b, the shifting direction changes to left. This result supports our conclusion that the FM1 layer dominate the current-driven magnetization switching process since the shifting tends to keep FM1 layer having magnetization direction along with the external magnetic field. In the low H_x range, the shifting with the different symmetry as described in the main body of our paper still exists, verifying that this shifting has different origin. In the third quadrant of the Figure S4a and the fourth quadrant of the Figure S4b, both the boundary lines have a sudden jump at $H_x = 800$ Oe, it probably originates from the formation of domains by the reversal of the out-of-plane component of the external magnetic field.

Section S3 The influence of thickness of Pt insert layer on H_{DM} .

It is hard to characterize the DM interaction in SAF structure directly, but we can measure the reference sample Ru(1)/Pt(50)/CoFe(0.41)/Pt(t_{Pt})/Ru(1.96)/Pt(2.3) without UM layer to investigate the influence of thickness of Pt insert layer on H_{DM} . Recently, Pai et al have develop a new method to measure the spin torque efficiency and DM interaction effective field H_{DM} . According to this method, under bias magnetic field and inject current I_{DC} along x axis, the $M-H_z$ loop in a SHE metal-based magnetic heterostructure will be shifted by H_{eff}^z , which represents the effective field generated by the current. The effective field generated per current density χ increases along with H_x until H_x finally overcome H_{DM} . In this method, steady depinning of domain wall rather than abrupt switching behaviour is desired to keep regular shift of the $M-H_z$ loops. To apply this method, we modified our electric magnet and added a powerful laser beam (650 nm, 300 mW) into the optical observing system. The laser beam is focused on the cross section of the Hall bar to induce heating effect as shown in Figure S6a. Under the heating the depinning of domain wall can be observed in the slant switching edge achieved for device with $t_{Pt} = 0.37$ nm shown in Figure S6b. H_{eff}^z show fine linearity along with I_{DC} , as shown in Figure S6c. Limited by the PMA of the sample, power of the electric magnet and the power of the laser, only χ values for $t_{Pt} = 0.45$ nm, 0.37 nm and 0.28 nm are shown in Figure S6(d - f). For $t_{Pt} = 0.45$ nm, it is obvious that $H_{DM} > 3000$ Oe since the χ is far away from saturation. When t_{Pt} decreases to 0.37 nm, a saturation trend can be found around $H_x = 2800$ Oe, but still a little too subtle since the saturation part is too short. For $t_{Pt} = 0.28$, however, the saturation point is more clear

and can be located around 2000 Oe. This trend of H_{DM} is quite interesting since in common idea the H_{DM} should decrease for better compensation of the Pt buffering and capping layer in Pt/Co/Pt structure. In our sample, the insert Pt layer is too thin to bring effective compensation, thus the change in interface condition is possibly the major contribution to the change in H_{DM} . Anyway, the H_{DM} measured in these devices have the same order with the estimated H_{DM} in main text, supporting our supposition on the role of DM interaction in the asymmetric switching.

Section S4 The energy barrier for nucleation increased by AFM coupling.

The formulas presented by Hellwig et al⁵ are used to estimate the influence of AFM coupling on the formation of domain in the respective of energy. Since the cycle of ferromagnetic layer in our work is $N = 2$, the energy of fully lateral correlation structure is given by

$$E_1 = 4\pi M_s^2 t - J_{\text{ex}} \quad (5)$$

where t is the sublayer thickness, M_s is the saturated magnetization and J_{ex} is the interlayer coupling strength across the Ru layer. We use the average thickness of the two sublayers, i.e. 0.46 for t , and the M_s is determined to be 1600 emu cm⁻³ by superconductor quantum interfere device (SQUID). Then J_{ex} is determined as 0.019 erg cm⁻² using the relation $J_{\text{ex}} = H_{\text{ex}} M_s t$. Then $E_1 = 1.46$ erg cm⁻². For a multidomain state, the energy E_2 have the expression depend on the magnetostatic energy E_{mag} and the domain wall energy E_{wall} and interlayer exchange energy

$$E_2 = E_{\text{mag}} + E_{\text{wall}} + J_{\text{ex}} \quad (6)$$

$$E_{\text{mag}} = \frac{16M_s^2 D^{\text{odd}}}{\pi^2} \sum_n \frac{1}{n^3} [1 - \exp(-2n\pi t/D)] \quad (7)$$

$$E_{\text{wall}} = \frac{8\sqrt{(AK_u)}t}{D} \quad (8)$$

where D is domain size, A is the atomic exchange ($\sim 10^{-6}$ erg cm) and K_u is the uniaxial perpendicular anisotropy constant. Corresponding to the initial domain obtained by current at low H_x , D is determined to be 1.6 μm . Averaged for the two sublayers, $K_u = 3.2 \times 10^6$ erg cm⁻³. The E_2 value of 1.50 is larger than E_1 , indicating the fully correlated AFM coupled state is energetically favoured than the multidomain

state. Notably that if all other parameter is fixed, the difference between these two states will not reverse until t exceeds 7.5 nm, implying the high stability of the AFM coupling. This difference increases the energy barrier for nucleation and then facilitate the asymmetric switching.

Supplementary References

- S1. U. H. Pi, K. W. Kim, J. Y. Bae, S. C. Lee, Y. J. Cho, K. S. Kim and S. Seo, *Appl. Phys. Lett.* , 2010, **97**.
- S2. S. Woo, M. Mann, A. J. Tan, L. Caretta and G. S. D. Beach, *Appl. Phys. Lett.* , 2014, **105**.
- S3. M. Hayashi, J. Kim, M. Yamanouchi and H. Ohno, *Phys. Rev. B*, 2014, **89**.
- S4. O. J. Lee, L. Q. Liu, C. F. Pai, Y. Li, H. W. Tseng, P. G. Gowtham, J. P. Park, D. C. Ralph and R. A. Buhrman, *Phys. Rev. B*, 2014, **89**.
- S5. O. Hellwig, T. L. Kirk, J. B. Kortright, A. Berger and E. E. Fullerton, *Nat. Mater.* , 2003, **2**, 112-116.

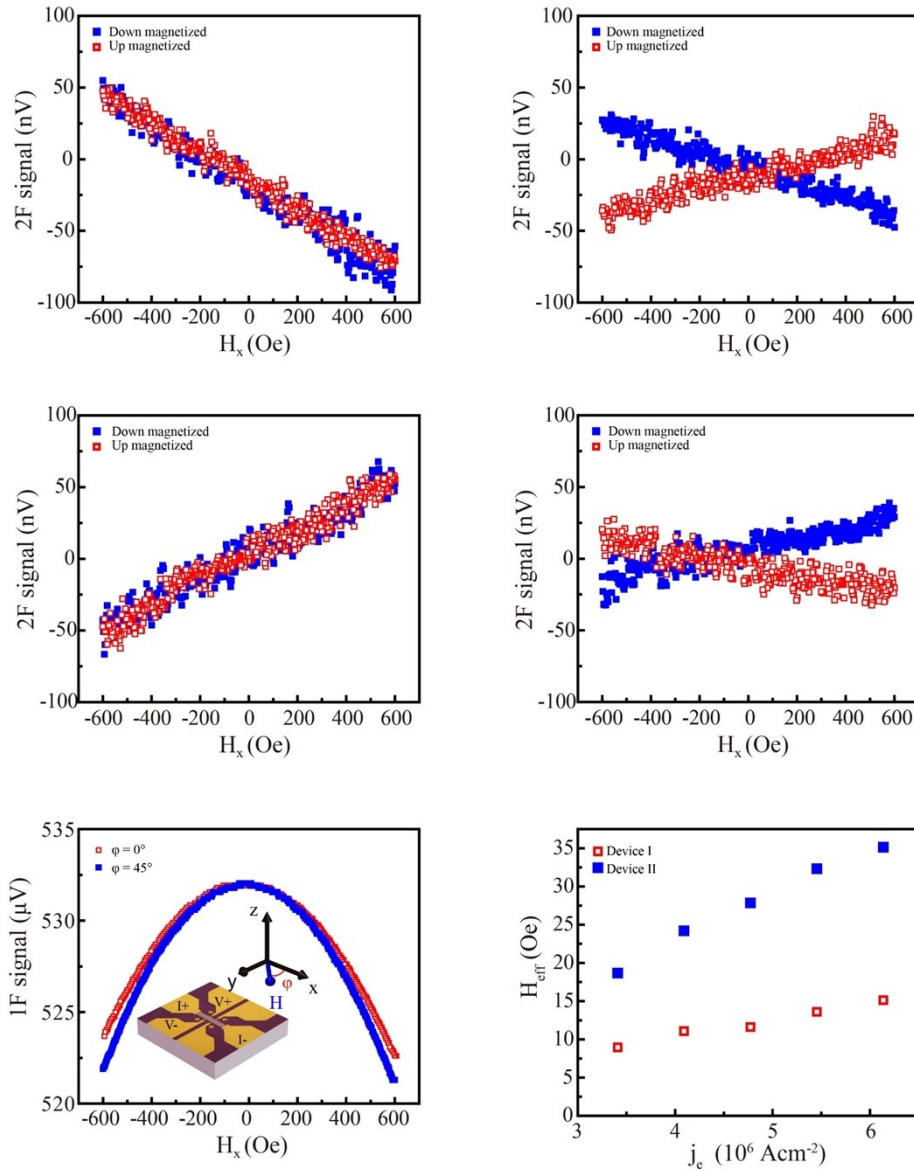


Figure S1 (a-d) Second harmonic signals of device I (a, b) and device II (c, d) under longitudinal magnetic field (a, c) and transverse field (b, d). (e) First harmonic signals versus in-plane applied field oriented at $\phi = 0^\circ$ (open square) and $\phi = 45^\circ$ (solid square) for device II. The inset indicates the geometry of the in-plane field. (f) Damping-like effective field versus current amplitude in device I (solid square) and device II (open square)

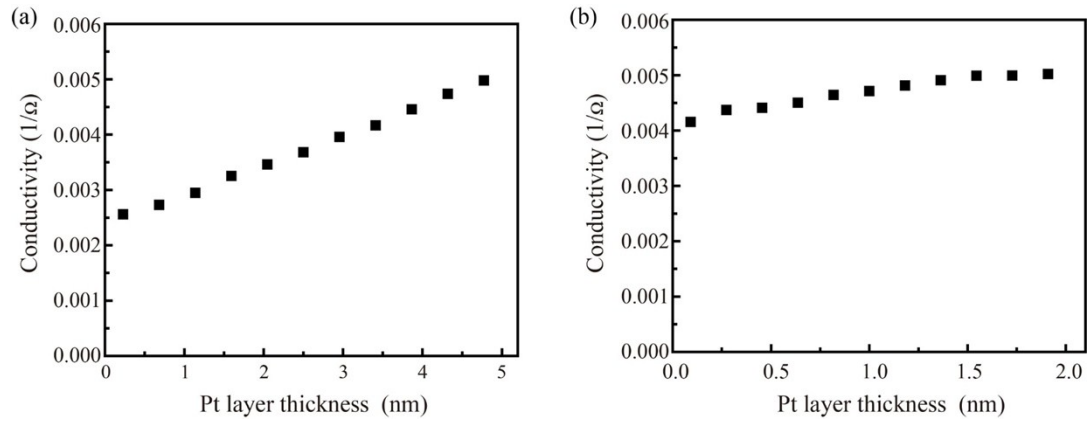


Figure S2 Channel conductivities of the Hall bars with the structure of **(a)** Ru(1)/Pt(0 - 5)/Co₇₀Fe₃₀(0.41)/Pt(0.27)/Ru(1.96)/Pt(0.27)/Co₇₀Fe₃₀(0.52)/Pt(2) and **(b)** Ru(1)Pt(5)/Co₇₀Fe₃₀(0.41)/Pt(0.27)/Ru(1.96)/Pt(0.27)/Co₇₀Fe₃₀(0.52)/Pt(0 - 2) (unit in nm).

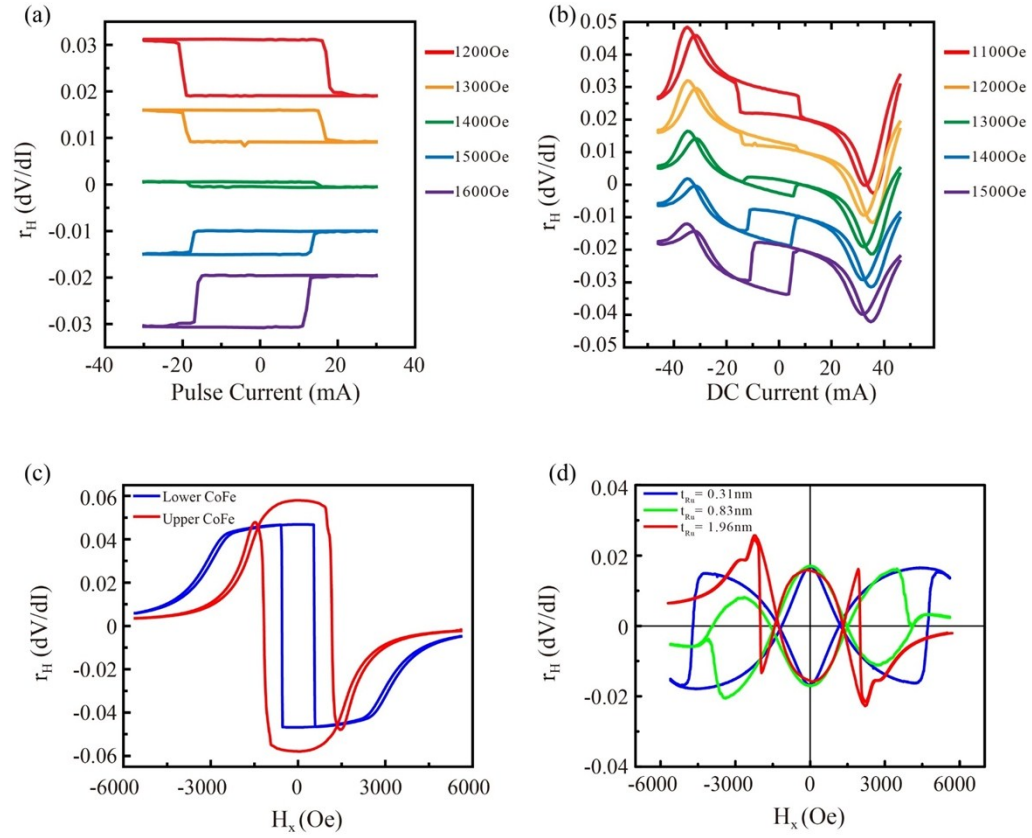


Figure S3 (a, b) The (a) pulse current driving switching loops and (b) d.c. current driving switching loops of the Hall bar of Ru(1)/Pt(5)/Co₇₀Fe₃₀(0.41)/Pt(0.27)/Ru(1.96)/Pt(0.27)/Co₇₀Fe₃₀(0.52)/Pt(2) (unit in nm) at different H_x . (c) r_H versus in-plane applied field for device I (blue) and device II (red) (d) r_H values of SAF structures with different t_{Ru} versus in-plane field.

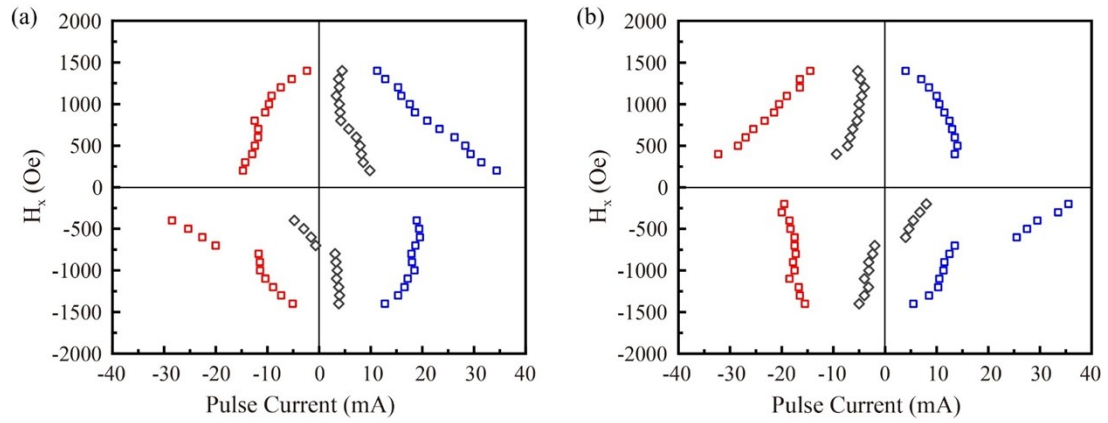


Figure S4 Switching phase diagrams measured under slightly tilted in-plane magnetic field with tilting angle (a) $\theta > 0$ and (b) $\theta < 0$. The red (blue) symbols indicate the I_{cri} values for switching towards up (down)-magnetized FM1 layer as indicated, while the gray symbols correspond to the average value of the boundaries.

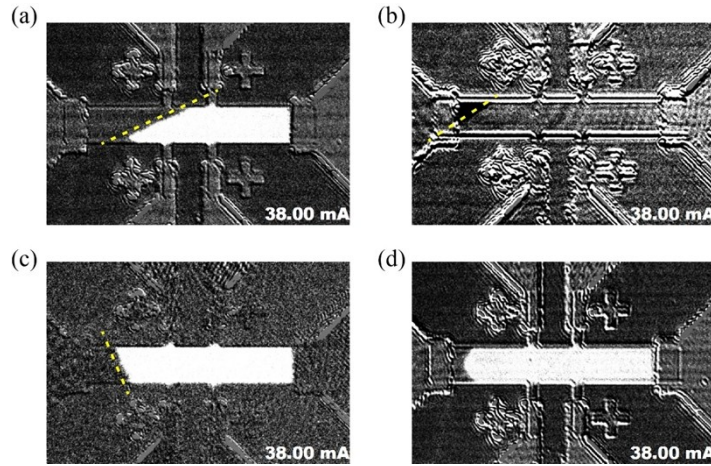


Figure S5 MOKE microscope images acquired at $H_x =$ (a) 500 Oe, (b) 600 Oe, (c) 800 Oe, and (d) 900 Oe after the same pulse current. The yellow dash lines indicate the location of the tilted straight domain wall. The Fig. S4(b) is darker than others because of the opposite magnetization direction of the image chosen for subtracting. It is clear that the tilting angle of the domain wall is continually decreasing along with increasing H_x . When H_x increases to 900 Oe, the domain wall does not have the sharp corner any more. With larger H_x , the magnetization is fully switched at current amplitude of 38 mA. This change from facet-like verifies that the competition between the Dzyaloshinskii-Moriya interaction and H_x is the main origin of the tilting domain wall.

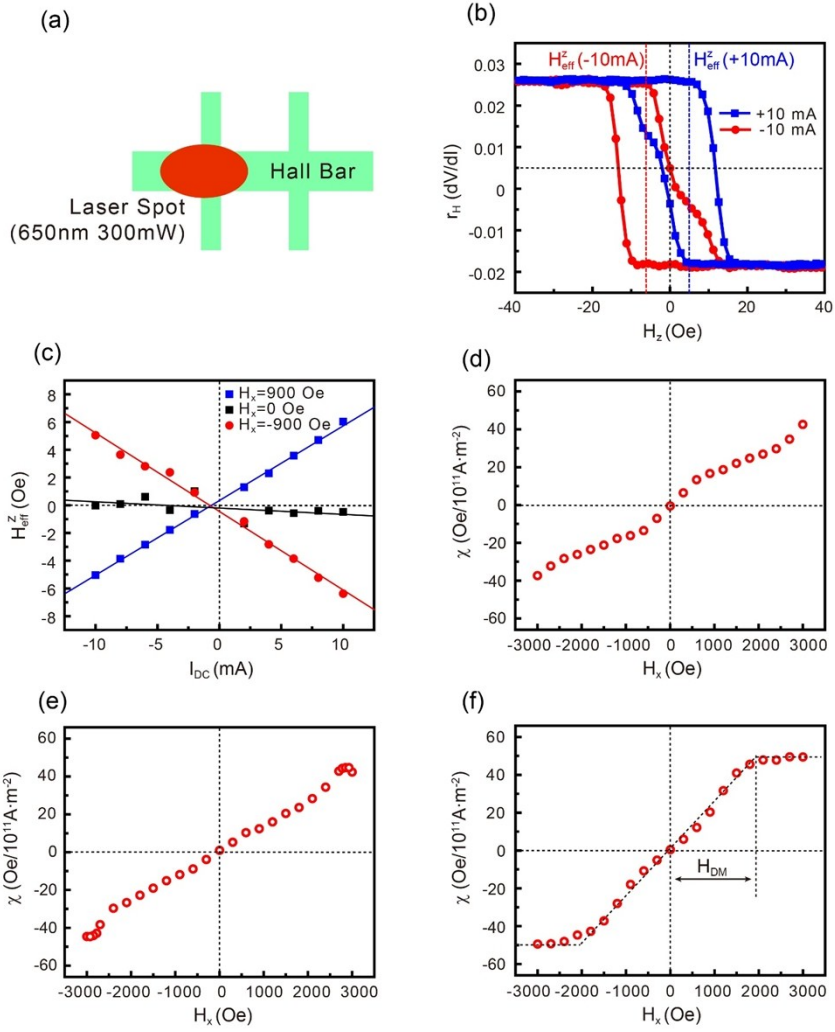


Figure S6 Measurement of H_{DM} for Ru(1)/Pt(50)/CoFe(0.41)/Pt(t_{Pt})/Ru(1.96)/Pt(2.3) (unit in nm). (a) The illustration of the laser spot for heating located at the cross section of the Hall bar. (b) $r_H - H_z$ loops for a $t_{Pt} = 0.37$ nm sample with dc current $I_{DC} = \pm 10$ mA and an in-plane bias field $H_x = 900$ Oe, H_{eff}^z represents the shift of the loops due to the spin-orbit torque. (c) H_{eff}^z for the same sample as a function of I_{DC} under $H_x = \pm 900$ Oe and 0 Oe. The solid lines are linear fits to the data. (d, e, f) The effective χ as a function of H_x for $t_{Pt} = 0.45$ nm (d), 0.37 nm (e) and 0.28 nm (f).

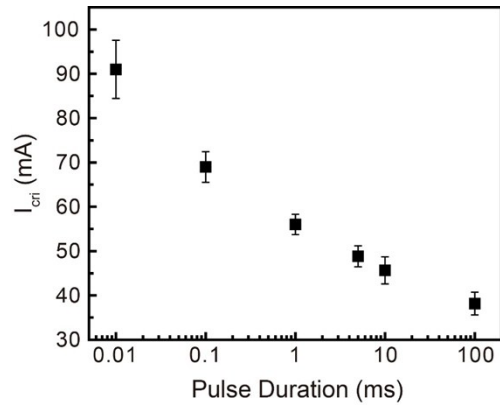


Figure S7 The critical current versus pulse duration for a SAF device measured at $H_x = 600$ Oe. By varying the duration of current pulse from 0.01 ms to 100 ms, it is obvious that shorter pulse need larger current value to complete the magnetization switching. This result indicates the heat generated by the current assists the switching process, coincident with the MOKE results. The value is larger than the origin devices in main text, thus, it is possibly because this new group of samples have larger H_{DM} .